Outer Van-Allen Radiation Belt Response to VLF Plasma Waves: Application of Granger Causality Method to Radiation Belt Storm Probe-A Data

Asif Shah (masifkf@gmail.com)
Theoretical Plasma Physics Division, PINSTECH, P.O. Nilore, Islamabad 44000 Pakistan

Research Article

Keywords: Granger causality analysis, Van-Allen radiation belts, very-low-frequency (VLF) waves, relativistic electrons flux, wave-particle interactions, radiation belt storm probes (RBSP) data.

Posted Date: May 16th, 2022

DOI: https://doi.org/10.21203/rs.3.rs-1651510/v1

Outer Van-Allen Radiation Belt Response to VLF Plasma Waves: Application of Granger Causality Method to Radiation Belt Storm Probe-A Data

Asif Shah

Theoretical Plasma Physics Division, PINSTECH, P.O. Nilore, Islamabad 44000 Pakistan

Abstract

Granger causality analysis is applied to very-low-frequency (VLF) waves and relativistic electrons interaction in an outer Van-Allen radiation belt. The VLF wave power and electrons flux data are one hour observations of radiation belt storm probe A (RBSP-A) during 14-3-2015. The considered VLF band comprises of 24 waves and electrons flux data at 8 pitch angles is considered. It is found that every wave is not Granger causing flux gradients for all pitch angles; rather some VLF waves are more efficient than others. Specifically, flux gradients at 69 degrees pitch angles are Granger caused by 14 kHz VLF wave. Contrarily, for 90 degrees pitch angles flux gradients are Granger caused by 6 waves. These results may be helpful for understanding the dynamics of outer radiation belt.

Key Words: Granger causality analysis, Van-Allen radiation belts, very-low-frequency (VLF) waves, relativistic electrons flux, wave-particle interactions, radiation belt storm probes (RBSP) data.

I. Introduction

The plasma particles (electrons, protons) trapping requires gradients parallel to the direction of magnetic field. This condition is naturally fulfilled by Earth's magnetic field, which is dipole-like up to few L-shells. Here L-shell represents the geocentric distance of a point

where magnetic field line intersects geomagnetic equator (that is 11 degrees tilted with respect to its geographic equator, for example L=2.5 means a point in magnetosphere that is lying on magnetic equator and is at distance of 2.5 Earth's radii from centre of Earth). In 1958, the first space mission (Explorer spacecraft) discovered two regions of trapped plasma in Earth's magnetosphere. These are known as Van-Allen radiation belts [1-2]. The inner radiation belt exists between L-shell= 1.5 – 3 and is mostly dominated by protons having energies 0.1 MeV – 40 MeV. The outer radiation belt occupies the region $4 < L\text{-shell} \lesssim 6.0$ and its electrons have energies in keV – MeV range. These radiation belts are separated by a slot region (L-shell=3-4), that is devoid of high intensity plasma particle radiations under normal conditions [3-4]. Electron fluxes in the outer radiation belt fluctuate by several orders of magnitude but its dynamics are yet not fully understood. Some intense storms can lead to the formation of a temporary third radiation belt (also known as storage ring) in slot region, which can survive for four weeks [5-6].

The space missions have confirmed the existence of many plasma waves in Earth's magnetosphere [7-12]. These include very-low-frequency (VLF) waves, which are whistler waves in frequency range 3-30 kHz [13-18], ultra-low-frequency (ULF) waves that are Alfven waves, electromagnetic ion cyclotron (EMIC) waves in vast frequency range (1Hz – 1mHz), their periods range from 1- 1000 seconds [19-20]. The VLF waves can be divided into two categories: upper band chorus (having frequencies $\leq 0.5\omega_c$ (cyclotron frequency)), and upper band chorus waves (with frequencies $> 0.5\ \omega_c$) [21].

The plasma particle sources of radiation belts include wave-particle interactions leading to radially inward diffusion of electrons. Wave-particle interactions also act as loss mechanism either by pitch angle scattering, or outward radial diffusion [22-29].

Many studies have focused on the wave-particle interactions in Van-Allen radiation belts and third radiation belt formation in slot region [26-29]. But the studies so far have not yet applied the Granger causality method to understand the relationship of VLF waves and outer radiation belt electrons pitch angle resolved flux. Therefore, this study for the first time applies Granger causality method to radiation belt storm probe A (RBSP) data of 24 VLF waves and 8 pitch angles resolved electrons flux. Using Granger causality method, this work finds answers to two basic research questions. The first research question states, do all 24 VLF waves in 10-30 kHz range have similar effects on outer radiation belt flux at pitch angles 16-90 degrees? The second research question states that, can VLF waves in frequency range 10-30 kHz non-resonantly affect the electrons flux? The answers for the first and second research questions are no, and yes respectively. The manuscript is organized as follows, section II is about data and methods. Section III describes the VLF plasma waves and electrons flux observations of radiation belt storm probe A (RBSP-A) for one hour. Section IV is devoted to the discussion of results by applying Granger Causality method. The summary of main findings is presented in section V.

II. Data and Methods

The VLF waves and electrons flux data analysed in this work are one hour observations of radiation belt storm probe A (RBSP-A) during 00:00:10.148 - 00:59:57.914, on 14-March-2015. The electrons flux data at 2 MeV energy and varying pitch angles from 16-90 degrees pitch angles and very-low-frequency (VLF) electric field power density data at 10 -30 kHz frequencies is analysed.

The flux data is from relativistic electron proton telescope (REPT), basically from NASA cdaweb (https://cdaweb.gsfc.nasa.gov/) at RBSP/ECT REPT pitch angle resolved electron

and proton fluxes with electron energies, 2-59.45 MeV with a logical source rbspa_rel03_ect-rept-l3. The time resolution of data values is varying from 10-11 seconds. The VLF waves power data comes from radio and plasma wave instrument (EMFISIS-L2, electric and magnetic field instrument level 2) with time resolution 6 seconds at http://rbsp-ect.sr.unh.edu.

The data file for Granger analysis is produced by selecting only those VLF power values which are almost simultaneous with the flux data. The gradients of flux are calculated by subtracting previous value of flux from its current value. A similar procedure is applied for calculating power density gradients in the time series for each of 24 VLF waves. The initial values of flux gradient and VLF power gradients are taken zero.

This work applies Granger causality tests to study the cause and effect relationship of 24 waves in very-low-frequency (VLF) band and 2 MeV relativistic electrons of outer Van-Allen radiation at 8 types of pitch angles.

The Granger causality test is a statistical procedure of hypothesis testing. There are two types of hypothesis: null and alternate. For this study, the null hypothesis states that temporal gradients of electrons flux time series at given pitch angle are independent of the temporal gradients in the power density time series of very-low-frequency electric field. Contrarily, the alternate hypothesis states that the temporal gradients of electrons flux time series are caused by the temporal gradients of VLF electric field power density gradients. Basically, there is not a single procedure to determine Granger causality. Different methods can be adopted to reject the null hypothesis and prove the causality of VLF waves and electrons flux. The lengthy details are avoided [already presented in Refs. 30, 31] here and a brief description is presented for readers. The causality judgement here is based on P-Value of F-statistics.

Basically, the formula of P-value reads as [30-31],

$$P - value = 1 - F^{cdf} \quad (1).$$

The superscript cdf in equation (1) indicates cumulative probability. However, F is calculated by the following relationship [30-31],

$$F = \frac{\left[\frac{SSR_r - SSR_u}{N_p}\right]}{\frac{SSR_u}{(N_0 - N_p - 1)}} \qquad (2)$$

Here SSR_r is sum square of residuals of the restricted model and SSR_u represent sum square of residuals of the un-restricted model, N_p is the number of predictor variables and N_0 is equal to the number of observations. This work takes a confidence interval of 95% which translates to a critical value of 0.05. When equation (1) returns a P-value less than 0.05, then null hypothesis is rejected and alternate hypothesis is accepted. Contrarily, when P-value is greater than 0.05 then null hypotheses is accepted and alternate hypothesis is rejected. Using this procedure the cause and effect relationships of the gradients in time series of VLF electric field power density and gradients in the time series of electrons flux are determined in figures (4)-(5) and explained in the discussion section IV.

III. Results

Figure 1 (a) displays the L-shell of radiation belt storm probe A with time. As the outer Van-Allen radiation belt exists between L = 4-6 and the L-shell of RBSP-A changed from L=5.8 to 6.4, therefore, the observations are at the outer edge of outer Van-Allen radiation belt and the findings of this study are more significant for understanding the relativistic electrons dynamics in the presence of VLF wave turbulence in that region of Earth's magnetosphere near geostationary orbit (at L=6.6).

The electrons in Van-Allen radiation belts can have three adiabatic invariants [33]. This study does not concentrate on the first and third adiabatic invariant and the figure 1 (b) displays second adiabatic invariant (SAI) for electrons. The SAI in figure 1(b) varied from 0.034 to 0.024. This indicates a 30 % reduction during the considered time interval. Based on this observation, SAI is not conserved for electrons. Under such conditions one cannot apply the adiabatic theory for finding the source of electrons flux changes. Although we have not provided the figure of first adiabatic invariant (FAI), but a simple argument indicates that FAI cannot be conserved. Because, the observed VLF waves frequencies (10-30 kHz) are comparable to the cyclotron frequencies of electrons (18.87 - 25.84 kHz) in the region of observations. This implies that the phase space density approach is also not applicable, because, it is only valid for conserved first adiabatic (FAI). Consequently, a new approach, Granger causality is adopted in this work to explore the influence of VLF waves on the relativistic electrons flux variations.

The power densities in 24 waves of very low frequency band are presented in the figures 2 (a)-(c). In figure 2(a) power densities for 8 types of VLF waves at frequencies 10.0, 10.5, 11.0, 11.5, 12.1, 12.7, 13.3, 14.0 kHz are presented. It shows that the highest power densities correspond to the 10 kHz waves and power density diminished as frequency increased, smallest power densities occurred for 14 kHz waves. The figure 2(b) displays the power densities for waves at 14.7, 15.4, 16.2, 17.0, 17.8, 18.7, 19.6, 20.5 kHz. Except 19.6, 20.5 these VLF waves have frequencies smaller than electron cyclotron and some of these can be recognized as lower band chorus waves when the criteria $f < 0.5f_c$ is satisfied. Here f and f_c denote wave frequency and an electron cyclotron frequency respectively. The VLF waves in figure 2(c) at frequencies 21.5, 22.6, 23.7, 24.9, 26.1, 27.4, 28.7, 30.1 kHz are upper band chorus waves, because these satisfy the criteria $f > 0.5f_c$.

Figure 3 (a) shows the scatter plot of the 2 MeV relativistic electrons flux at 8 pitch angles, 16, 26, 37, 47, 58, 69, 79, and 90 degrees. The flux is decreasing with the time for electrons at these considered pitch angles. To highlight extra information, figure 3 (b) presents a contour plot of the 2 MeV relativistic electrons with time and pitch angles. The highest flux peaks occurred for 37 degrees and 47 degrees pitch angles. Temporal trend shows that flux at all pitch angles is diminishing with time. The presence of VLF waves in figures 2 and flux changes in figure (3) can be linked together. One can assume that flux changes in figure (3) are due to VLF wave interactions with electrons. Such possibilities are explained in the following section.

IV. Discussion of Results:

Radiation belt storm probe A (RBSP-A) simultaneously observed VLF waves (figure 2) and relativistic electrons flux reduction (figure 3), this implies that the flux changes are triggered by VLF waves. However, there are some basic research questions, such as, are the electron flux changes at 16 degrees pitch angles are caused by all the 24 waves or by only one wave? Similar, research questions can be asked for electrons flux changes at other pitch angles and combinations of waves. The RBSP-A observations in figures (2) and (3) cannot provide answers to such research questions. Therefore, further analysis of data in figures (2) and (3) is required. This work applies the Granger causality tests to explore the roles of considered VLF waves. The critical value 0.05 is used for judgement. When P-value is smaller than 0.05, then we reject the null hypothesis and alternate hypothesis is accepted. Otherwise, when P-value is greater than 0.05, then null hypothesis is accepted and alternate hypothesis is rejected. In this study, the null hypothesis states, the electron flux gradients at pitch angle (= 16, 26, 37, 47, 58, 69, 79, 90 degrees) are independent of the gradients in powers of VLF wave (10, 10.5,

11.0, 11.5, 12.1, 12.7, 13.3, 14.0, 14.7, 15.4, 16.2, 17.0, 17.8, 18.7, 19.6, 20.5, 21.5, 22.6, 23.7, 24.9, 26.1, 27.4, 28.7, 30.1 kHz). The alternate hypothesis states that flux gradients are dependent on the gradients of the wave power. These hypotheses are tested with Granger causality test and relationships between waves and flux changes at considered frequencies, and pitch angles are determined. Figure 4 shows P-values of Granger causality tests at 4-lags for the 2 MeV electrons at pitch angles 58 degrees (4a), 69 degrees (4b), 79 degrees (4c), and 90 degrees (4d). In figures 4 (a) –(d) the horizontal red line shows a critical level of 0.05 and any point that lies under this level leads to rejection of null hypotheses and all points above it, accepts the null hypothesis. The P-values in figure 4(a) show that 8 waves Granger caused the flux changes for 58 degrees pitch angle electrons. Contrarily, gradients in power of only one wave (at 14 kHz) Granger caused (resulted in P-values less than 0.05 for first and second lag) flux gradients at 69 degrees pitch angles, as shown in figure 4(b). The flux changes in figure 4 (c) for 79 degrees pitch angle electrons are Granger caused by two waves. Figure 4 (d) shows that power gradients of 6 waves Granger caused flux variations of 90 degrees pitch angle electrons. Figure 5 shows that the flux gradients of 16 (figure 5a), 26 (figure 5b), 37 (figure 5c), and 47 degrees (figure 5d) pitch angle electrons are Granger caused by 2, 5, 3, and 5 waves respectively. The results in figures (4) and (5) also suggest that VLF waves also interact non-resonantly with outer Van-Allen radiation belt electrons, because, all these waves does not satisfy the cyclotron resonance condition. For example, consider the case of 90 degrees pitch angle in figure 4 (d). In this case, 18.87 kHz VLF wave frequency is comparable to electron cyclotron frequency (18.87 - 25.84 kHz) in region of observation, therefore, the flux changes due 18.87 kHz VLF wave can be recognized as cyclotron resonant effect. Because, the cyclotron resonance condition reads [32-33],

$$\omega - kV_{Parll} = n\omega_c \quad (3).$$

For 90 degrees pitch angle, parallel velocity $V_{Parll} = 0$, and resonance condition (1) reduces to $\omega = \omega_c$ when $n = 1$. The effects of 20.5, 23.7 kHz waves can also be attributed to cyclotron resonance for $n = 1$ because, these waves are bounded in the domain of electron cyclotron frequencies (18.87 - 25.84 kHz). However, the VLF waves at 12.1, 27.4 kHz and 28.7 kHz does not satisfy the resonance condition for any n ($= \pm 1, \pm 2, \pm 3, ...$) and therefore, these waves non-resonantly Granger caused flux gradients for the 90 degrees pitch angle electrons.

V. Summary and Conclusions:

The radiation belt storm probe (RBSP-A) simultaneous observations of 24 VLF waves and diminishing fluxes of 2 MeV electrons at 8 pitch angles suggest that flux changes may be due to VLF waves. By applying, the Granger causality tests, we find an answer to the basic research question, does all 24 VLF waves equally contributed to electrons flux changes? The answer is that all these waves do not contribute equally to electron flux changes in outer radiation belt at the considered pitch angles. This work also answers another research question, does VLF wave only Granger caused flux gradients when cyclotron resonance condition is satisfied. It is found that in some cases flux changes are Granger caused by VLF waves satisfying cyclotron resonance condition but not always. This implies that VLF waves also interacted non-resonantly with electrons and caused flux changes. The findings of this study can be helpful for understanding the dynamics of outer radiation belt.

Acknowledgement: The author is thankful to NASA cdaweb and D.N. Baker for REPT measured electrons flux data. We are also thankful to C. Kletzing for EMFISIS-L2 data of VLF wave electric field power density data.

Data availability statement: The data is available upon request to corresponding author at masifkf@gmail.com.

Conflict of Interest: The author has no conflict of interest.

References

[1]Van Allen, J. A., & Frank, L. A. Radiation Around the Earth to a Radial Distance of 107,400 km. *Nature* **183**, 430-434 (1959).

[2]Van Allen, J. A. Radiation belts around the Earth. *Scientific American*, ***200,*** 39-47 (1959).

[3]Summers, D., Mann, I. R., Baker, D. N., & Schulz, M. G. (Eds.). (2013). *Dynamics of the Earth's radiation belts and inner magnetosphere* (Vol. 199). John Wiley & Sons.

[4]Friedel, R. H. W., G. D. Reeves, and T. Obara. Relativistic electron dynamics in the inner magnetosphere—A review. *Journal of Atmospheric and Solar-Terrestrial Physics* **64**, 265-282 (2002).

[5]Baker, D.N., Kanekal, S.G., Hoxie, V.C., Henderson, M.G., Li, X., Spence, H.E., Elkington, S.R., Friedel, R.H.W., Goldstein, J., Hudson, M.K. and Reeves, G.D., 2013. A long-lived relativistic electron storage ring embedded in Earth's outer Van Allen belt. *Science*, *340*(6129), pp.186-190.

[6]Shprits, Y.Y., Subbotin, D., Drozdov, A., Usanova, M.E., Kellerman, A., Orlova, K., Baker, D.N., Turner, D.L. and Kim, K.C., 2013. Unusual stable trapping of the ultrarelativistic electrons in the Van Allen radiation belts. *Nature Physics*, *9*(11), pp.699-703.

[7]LaBelle, J. and Treumann, R.A., 1988. Plasma waves at the dayside magnetopause. *Space Science Reviews*, *47*(1), pp.175-202.

[8]Shawhan, S.D., 1979. Magnetospheric plasma wave research 1975–1978. *Reviews of Geophysics*, *17*(4), pp.705-724.

[9]Shawhan, S.D., 1977. *Magnetospheric plasma waves* (No. TRITA-EPP--77-07). Kungliga Tekniska Hoegskolan.

[10]Yumoto, K., 1988. External and internal sources of low-frequency MHD waves in the magnetosphere-A review. *Journal of geomagnetism and geoelectricity*, *40*(3), pp.293-311.

[11]Amatucci, W.E., 2006. A review of laboratory investigations of space plasma waves. *URSI Radio Science Bulletin*, *2006*(319), pp.32-66.

[12]Lanzerotti, L.J., Fukunishi, H., Maclennan, C.G. and Cahill Jr, L.J., 1976. Observations of magnetohydrodynamic waves on the ground and on a satellite. *Journal of Geophysical Research*, *81*(25), pp.4537-4545.

[13]Hashimoto, Kozo, Isamu Nagano, Masayuki Yamamoto, Toshimi Okada, Iwane Kimura, Hiroshi Matsumoto, and Hidetaka Oki. "EXOS-D (AKEBONO) very low frequency plasma wave instruments (VLF)." *IEEE transactions on geoscience and remote sensing* 35, no. 2 (1997): 278-286.

[14]Cohen, M. (2013, May). Very Low Frequency Remote Sensing of the Ionosphere and Magnetosphere. In *AGU Spring Meeting Abstracts* (Vol. 2013, pp. SM24A-01).

[15]Kaiser, T. R., D. Orr, and A. J. Smith. "Very low frequency electromagnetic phenomena:‘whistlers’ and micropulsations." *Philosophical Transactions of the Royal Society of London. B, Biological Sciences* 279, no. 963 (1977): 225-238.

[16]Záhlava, J., F. Němec, Jean-Louis Pincon, O. Santolík, I. Kolmašová, and Michel Parrot. "Whistler influence on the overall very low frequency wave intensity in the upper ionosphere." *Journal of Geophysical Research: Space Physics* 123, no. 7 (2018): 5648-5660.

[17]Sazhin, S. S. "VLF emissions in the earth's magnetosphere." *Geomagnitnye Issledovaniia* 18 (1976): 24-53.

[18]Kulkarni, V. H., and Jharana Das. "Very low frequency (VLF) chorus emissions: A topical survey." *Surveys in geophysics* 13, no. 1 (1992): 35-46.

[19]Dungey, J. W., & Southwood, D. J. (1970). Ultra-low frequency waves in the magnetosphere. *Space Science Reviews*, *10*(5), 672-688.

[20]Menk, F. W. (2011). Magnetospheric ULF waves: A review. *The dynamic magnetosphere*, 223-256.

[21]Sazhin, S. S., and M. Hayakawa. "Magnetospheric chorus emissions: A review." *Planetary and space science* 40, no. 5 (1992): 681-697.

[22]Rae, I.J., Murphy, K.R., Watt, C.E., Halford, A.J., Mann, I.R., Ozeke, L.G., Sibeck, D.G., Clilverd, M.A., Rodger, C.J., Degeling, A.W. and Forsyth, C., 2018. The role of localized compressional ultra-low frequency waves in energetic electron precipitation. *Journal of Geophysical Research: Space Physics*, *123*(3), pp.1900-1914.

[23]Su, Z., Zhu, H., Xiao, F., Zong, Q.G., Zhou, X.Z., Zheng, H., Wang, Y., Wang, S., Hao, Y.X., Gao, Z. and He, Z., 2015. Ultra-low-frequency wave-driven diffusion of radiation belt relativistic electrons. *Nature communications*, *6*(1), pp.1-8.

[24]Rankin, R., Wang, C.R., Wang, Y.F., Zong, Q., Zhou, X.Z., Degeling, A.W., Sydorenko, D. and Whittall-Scherfee, G., 2020. Ultra-Low-Frequency Wave–Particle Interactions in Earth's Outer Radiation Belt. *Dayside Magnetosphere Interactions*, pp.189-205.

[25]Zong, Q., Hao, Y. and Wang, Y., 2009. Ultra low frequency waves impact on radiation belt energetic particles. *Science in China Series E: Technological Sciences*, *52*(12), pp.3698-3708.

[26]Thorne, R.M., 2010. Radiation belt dynamics: The importance of wave-particle interactions. *Geophysical Research Letters*, *37*(22).

[27]Watt, C.E., Rae, I.J., Murphy, K.R., Anekallu, C., Bentley, S.N. and Forsyth, C., 2017. The parameterization of wave-particle interactions in the Outer Radiation Belt. *Journal of Geophysical Research: Space Physics*, *122*(9), pp.9545-9551.

[28]Xiao, F., Liu, S., Tao, X., Su, Z., Zhou, Q., Yang, C., He, Z., He, Y., Gao, Z., Baker, D.N. and Spence, H.E., 2017. Generation of extremely low frequency chorus in Van Allen radiation belts. *Journal of Geophysical Research: Space Physics*, *122*(3), pp.3201-3211.

[29]Allison, H.J., Shprits, Y.Y., Zhelavskaya, I.S., Wang, D. and Smirnov, A.G., 2021. Gyroresonant wave-particle interactions with chorus waves during extreme depletions of plasma density in the Van Allen radiation belts. *Science advances*, *7*(5), p.eabc0380.

[30]Shojaie, Ali, and Emily B. Fox. "Granger causality: A review and recent advances." *Annual Review of Statistics and Its Application* 9 (2022): 289-319.

[31]Faes, L., Nollo, G., Stramaglia, S., & Marinazzo, D. (2017). Multiscale granger causality. *Physical Review E*, *96*(4), 042150.

[32]Litvak, A.G., Sergeev, A.M., Suvorov, E.V., Tokman, M.D. and Khazanov, I.V., 1993. On nonlinear effects in electron-cyclotron resonance plasma heating

by microwave radiation. *Physics of Fluids B: Plasma Physics*, *5*(12), pp.4347-4359.

[33]Baumjohann, W., & Treumann, R. A. (2012). *Basic space plasma physics (revised edition)*. World Scientific Publishing Company.

Figure Captions

Figure 1 shows (a) L-shell of radiation belt storm probe A (RBSP-A) during one hour observations (00:00:10.148 - 00:59:57.914) on 14-March-2015. (b) Exhibits temporal variations in the electrons second adiabatic invariant.

Figure 2 shows very- low-frequency (VLF) waves electric field power densities for (a) eight waves at 10.0, 10.5, 11.0, 11.5, 12.1, 12.7, 13.3, 14.0 kHz (b) eight waves at 14.7, 15.4, 16.2, 17.0, 17.8, 18.7, 19.6, 20.5 kHz (c) eight waves at 21.5, 22.6, 23.7, 24.9, 26.1, 27.4, 28.7, 30.1 kHz. These are observations of RBSP-A for same time interval as in figure 1.

Figure 3 shows (a) scatter plot of 2 MeV energy electrons pitch angle resolved flux at eight pitch angles, 16, 26, 37, 47, 58, 69, 79, 90 degrees respectively (b) displays contour plot of the 2 MeV electrons flux with pitch angle and time. The flux measurements are based on the relativistic electron proton telescope (REPT) on board RBSP-A during one hour observations (00:00:10.148 - 00:59:57.914) on 14-March-2015.

Figure 4 shows the P-values of Granger causality test, determined for gradients in VLF waves powers and gradients of electrons flux at pitch angles (a) 58 degrees (b) 69 degrees (c) 79 degrees, and (d) 90 degrees. When P-value is less than critical value 0.05 (highlighted with red horizontal line) then null hypothesis is rejected and flux gradients are Granger caused by power gradients of VLF waves. Otherwise, null hypothesis is accepted and flux gradients are thought to be independent of power gradients of VLF wave.

Figure 5 shows the P-values of Granger causality test determined for gradients in VLF waves powers and gradients of electrons flux at pitch angles (a) 16 degrees (b) 26 degrees (c) 37 degrees, and (d) 47 degrees.

Figure 1

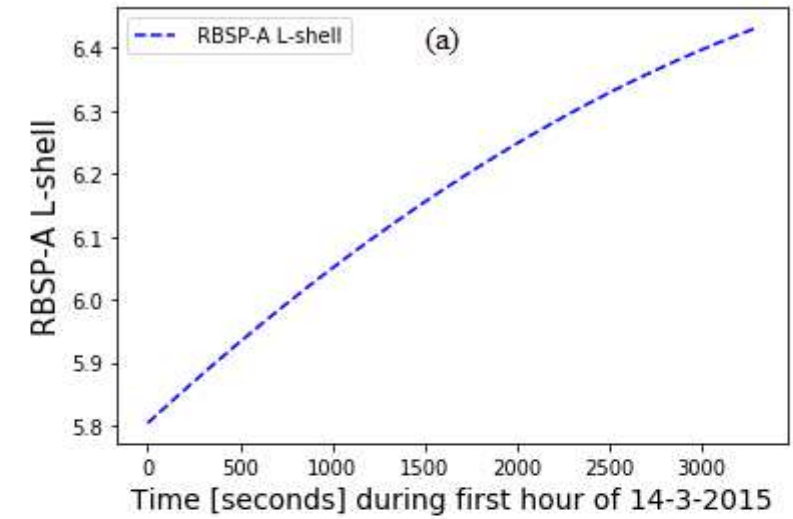
RBSP-A L-shell
(a)
RBSP-A L-shell
6.4
6.3
6.2
6.1
6.0
5.9
5.8
0
500
1000
1500
2000
2500
3000
Time [seconds] during first hour of 14-3-2015

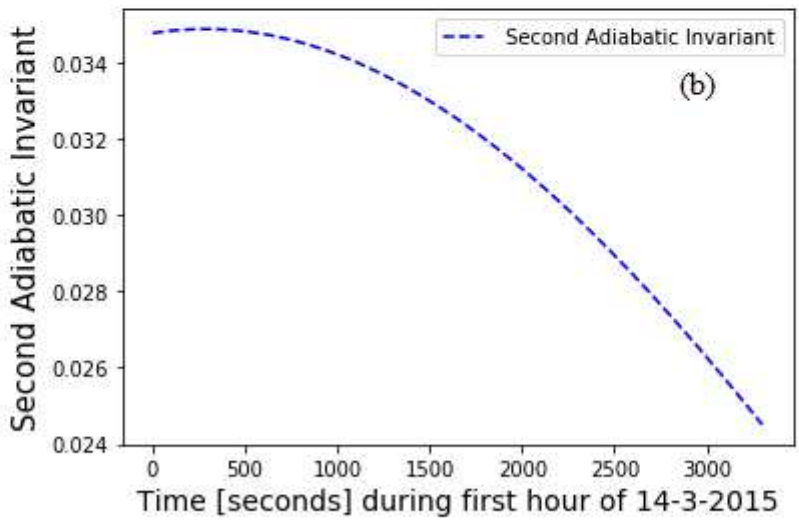
Second Adiabatic Invariant
(b)
Second Adiabatic Invariant
0.034
0.032
0.030
0.028
0.026
0.024
0
500
1000
1500
2000
2500
3000
Time [seconds] during first hour of 14-3-2015

Figure 2

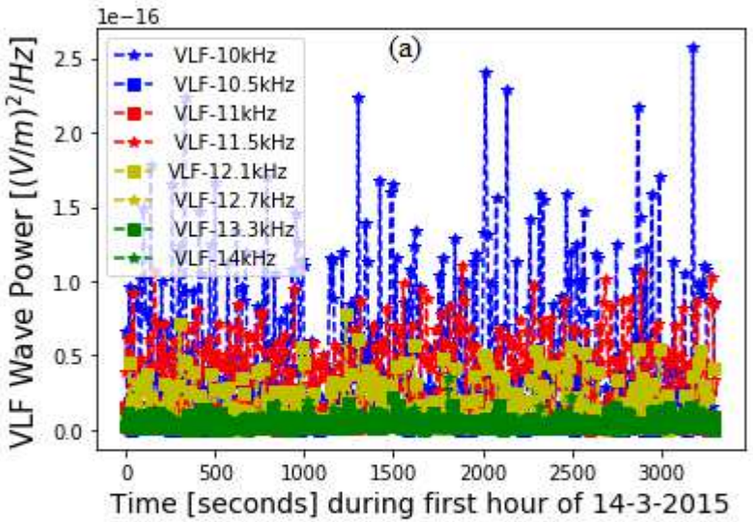
1e−16
(a)
VLF-10kHz
VLF-10.5kHz
VLF-11kHz
VLF-11.5kHz
VLF-12.1kHz
VLF-12.7kHz
VLF-13.3kHz
VLF-14kHz
VLF Wave Power [(V/m)²/Hz]
Time [seconds] during first hour of 14-3-2015

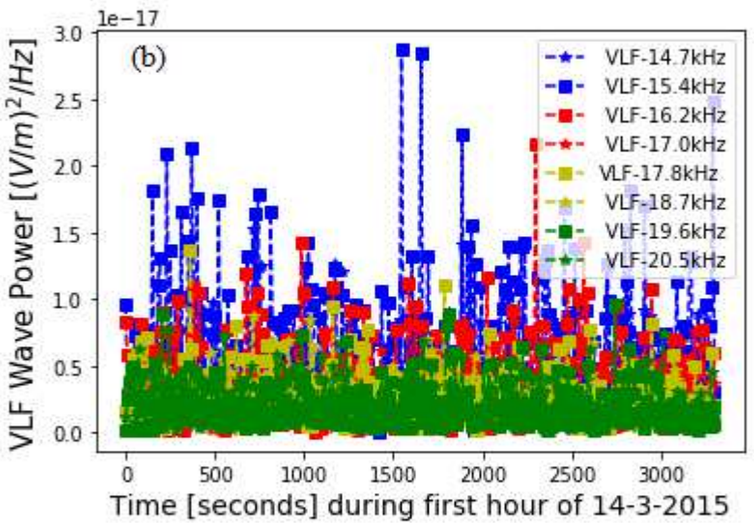
1e−17
(b)
VLF-14.7kHz
VLF-15.4kHz
VLF-16.2kHz
VLF-17.0kHz
VLF-17.8kHz
VLF-18.7kHz
VLF-19.6kHz
VLF-20.5kHz
VLF Wave Power [(V/m)²/Hz]
Time [seconds] during first hour of 14-3-2015

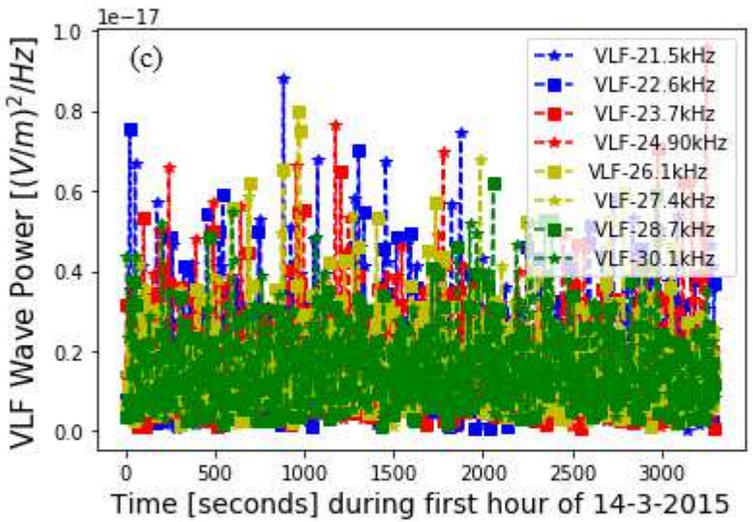
1e−17
(c)
VLF-21.5kHz
VLF-22.6kHz
VLF-23.7kHz
VLF-24.90kHz
VLF-26.1kHz
VLF-27.4kHz
VLF-28.7kHz
VLF-30.1kHz
VLF Wave Power [(V/m)²/Hz]
Time [seconds] during first hour of 14-3-2015

Figure 3

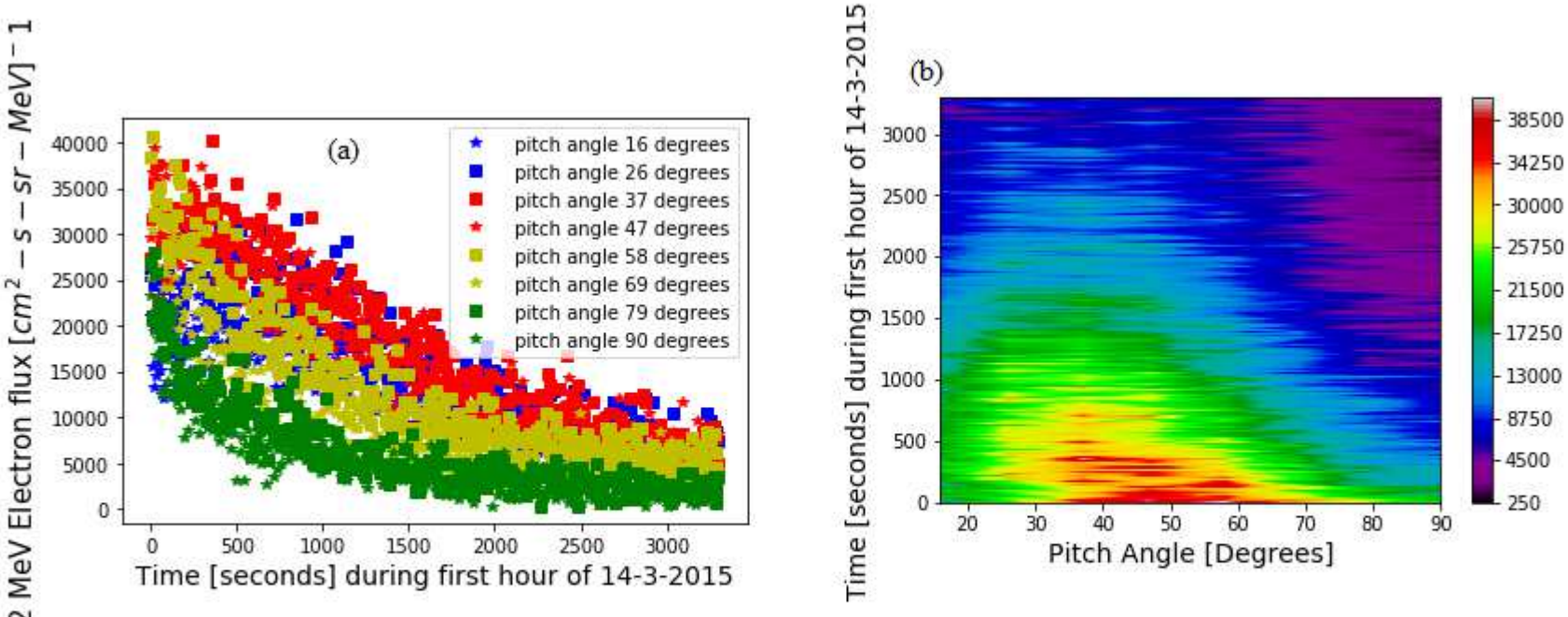
(a)
pitch angle 16 degrees
pitch angle 26 degrees
pitch angle 37 degrees
pitch angle 47 degrees
pitch angle 58 degrees
pitch angle 69 degrees
pitch angle 79 degrees
pitch angle 90 degrees
2 MeV Electron flux [cm^2 − s − sr − MeV] − 1
Time [seconds] during first hour of 14-3-2015
(b)
Time [seconds] during first hour of 14-3-2015
Pitch Angle [Degrees]

Figure 4

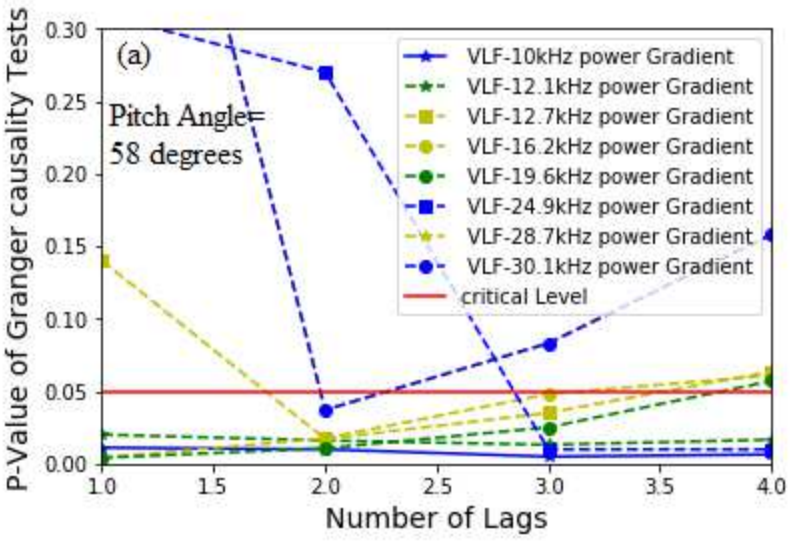
(a)
Pitch Angle=
58 degrees
VLF-10kHz power Gradient
VLF-12.1kHz power Gradient
VLF-12.7kHz power Gradient
VLF-16.2kHz power Gradient
VLF-19.6kHz power Gradient
VLF-24.9kHz power Gradient
VLF-28.7kHz power Gradient
VLF-30.1kHz power Gradient
critical Level
P-Value of Granger causality Tests
Number of Lags

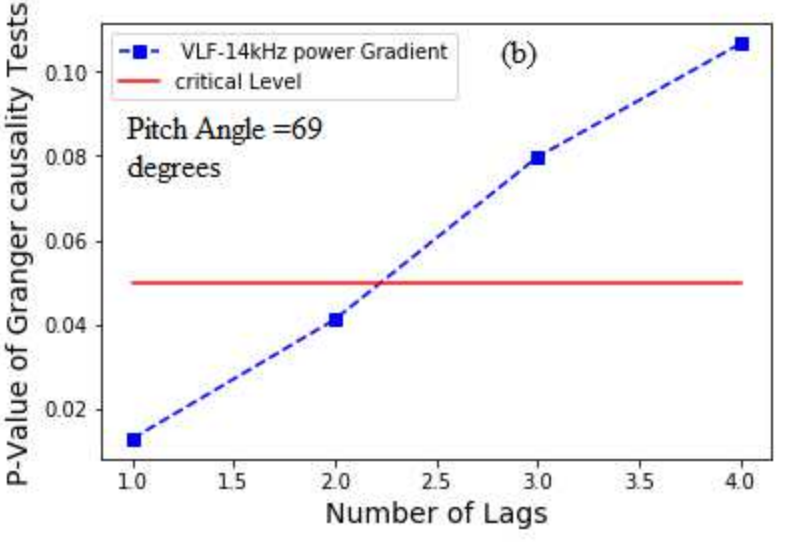
(b)
Pitch Angle =69
degrees
VLF-14kHz power Gradient
critical Level
P-Value of Granger causality Tests
Number of Lags

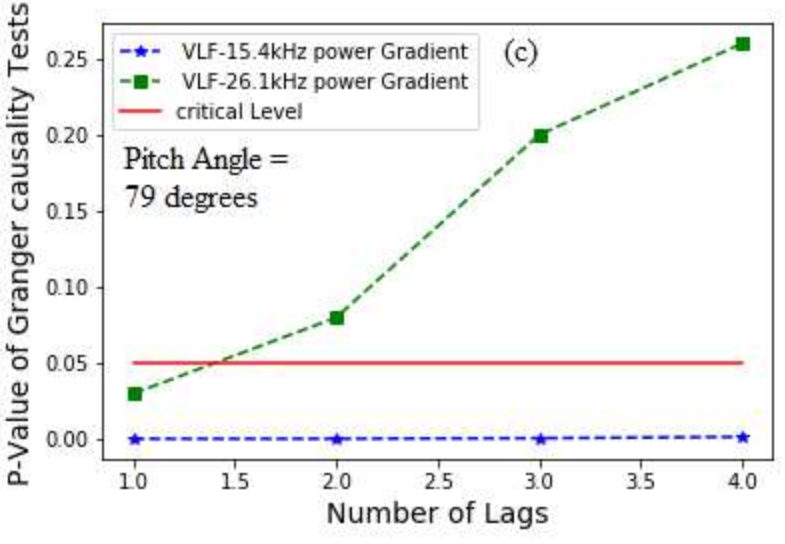
(c)
Pitch Angle =
79 degrees
VLF-15.4kHz power Gradient
VLF-26.1kHz power Gradient
critical Level
P-Value of Granger causality Tests
Number of Lags

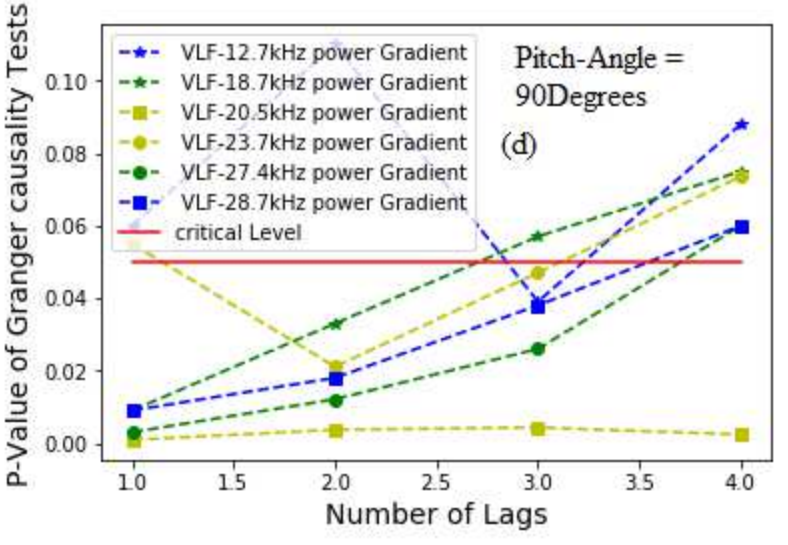
(d)
Pitch-Angle =
90Degrees
VLF-12.7kHz power Gradient
VLF-18.7kHz power Gradient
VLF-20.5kHz power Gradient
VLF-23.7kHz power Gradient
VLF-27.4kHz power Gradient
VLF-28.7kHz power Gradient
critical Level
P-Value of Granger causality Tests
Number of Lags

Figure 5

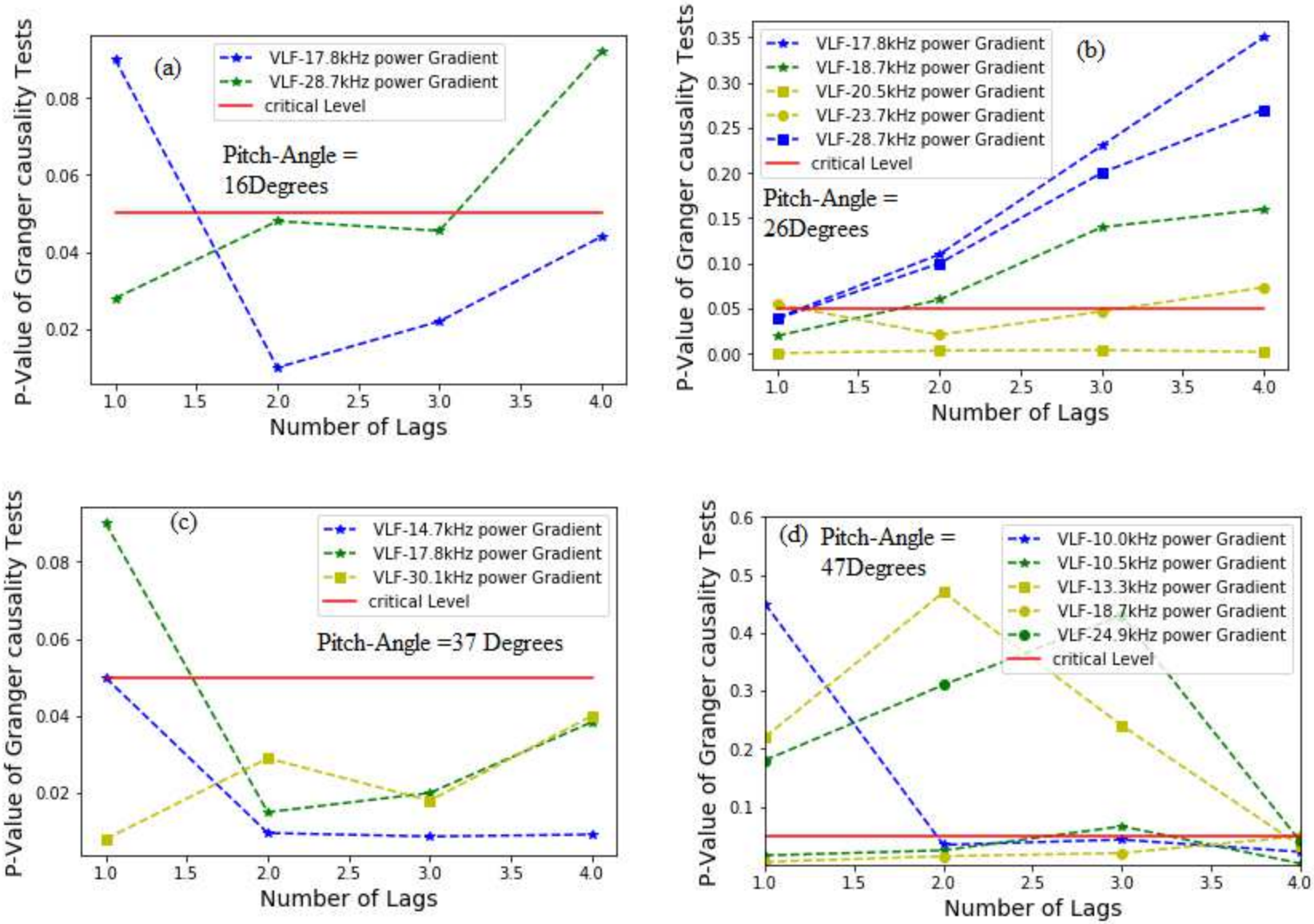
(a)
VLF-17.8kHz power Gradient
VLF-28.7kHz power Gradient
critical Level
Pitch-Angle = 16Degrees
P-Value of Granger causality Tests
Number of Lags
(b)
VLF-17.8kHz power Gradient
VLF-18.7kHz power Gradient
VLF-20.5kHz power Gradient
VLF-23.7kHz power Gradient
VLF-28.7kHz power Gradient
critical Level
Pitch-Angle = 26Degrees
P-Value of Granger causality Tests
Number of Lags
(c)
VLF-14.7kHz power Gradient
VLF-17.8kHz power Gradient
VLF-30.1kHz power Gradient
critical Level
Pitch-Angle =37 Degrees
P-Value of Granger causality Tests
Number of Lags
(d) Pitch-Angle = 47Degrees
VLF-10.0kHz power Gradient
VLF-10.5kHz power Gradient
VLF-13.3kHz power Gradient
VLF-18.7kHz power Gradient
VLF-24.9kHz power Gradient
critical Level
P-Value of Granger causality Tests
Number of Lags